Tectonics

RESEARCH ARTICLE
10.1029/2017TC004940

Special Section:
Geodynamics, Crustal and Lithospheric Tectonics, and active deformation in the Mediterranean Regions (A tribute to Prof. Renato Funiciello)

The Dewatering of the Fucino Lake Did Not Promote the *M*7.1 1915 Fucino Earthquake: Insights From Numerical Simulations

L. Cucci[1], **G. Currenti**[2], **M. Palano**[2], **and A. Tertulliani**[1]

[1]Sezione di Sismologia e Tettonofisica, Istituto Nazionale di Geofisica e Vulcanologia, Rome, Italy, [2]Sezione di Catania—Osservatorio Etneo, Istituto Nazionale di Geofisica e Vulcanologia, Catania, Italy

Abstract The powerful *M*7.1 earthquake that devastated the Fucino Basin (Central Italy) in 1915 results to be the only (except for a *M*5.7 event in 1904) remarkable event to have occurred in that area, according to the 900-year-long record of the Italian Seismic Catalogue. Curiously, the 1915 event occurred only 38 years after the complete man-induced dewatering of the largest lake of peninsular Italy, which formerly occupied the basin. Hence, we investigate on a possible relationship between the dewatering of the lake and the occurrence of the 1915 earthquake. We perform some numerical simulations in order to estimate the stress changes induced by the dewatering of the Fucino Lake and by the 1904 earthquake. We compute the stress changes on two different seismogenic sources selected among the ones proposed in the literature. Our main results support that (1) the dewatering process has reduced effects of the state of stress in the area before the 1915 earthquake, (2) the primary effect of the dewatering on both sources is a decrease of stresses that hampers the slip on the fault planes, and (3) the positive stress changes associated to the 1904 event would be too weak to influence the occurrence of the 1915 earthquake. We also suggest that the dewatering may have delayed by ~1.7 years the 1915 earthquake occurrence.

Plain Language Summary The powerful *M*7.1 earthquake that devastated the Fucino Basin (Central Italy) in 1915 occurred only 38 years after the complete man-induced dewatering of the largest lake of peninsular Italy, which formerly occupied the basin. Hence, we investigate on a possible relationship between the dewatering of the lake and the occurrence of the 1915 earthquake. We find that the stress changes originated by the Fucino Lake dewatering represent the main factor of perturbation in the area prior to 1915; however, such a dewatering process may have only slightly (a couple of years) delayed the occurrence of the strong rupture of the 1915 earthquake. Our work confirms the possibility that human activities can induce a temporal delay in the occurrence of future earthquakes.

Key Points:
- The dewatering of the Fucino Lake may have slightly delayed the occurrence of the strong rupture of the 1915 earthquake
- The Coulomb stress changes originated by the dewatering are the main perturbation factor of the state of stress in the area prior to 1915
- Human activities can induce a temporal delay in the occurrence of future earthquakes

Supporting Information:
- Supporting Information S1

Correspondence to:
L. Cucci,
luigi.cucci@ingv.it

Citation:
Cucci, L., Currenti, G., Palano, M., & Tertulliani, A. (2018). The dewatering of the Fucino Lake did not promote the *M*7.1 1915 Fucino earthquake: Insights from numerical simulations. *Tectonics*, *37*. https://doi.org/10.1029/2017TC004940

Received 22 DEC 2017
Accepted 6 JUL 2018
Accepted article online 13 JUL 2018

1. Introduction

In the last decades, a number of studies have pointed out how surface/subsurface crustal (un)loading can influence stress perturbations thereby promoting fault slip in different tectonic contexts. Valuable examples come from reservoir impoundment (e.g., Gupta, 2002; Hua et al., 2015; Kebeasy & Gharib, 1991; Tuan et al., 2017), groundwater extraction (e.g., Amos et al., 2014; Gonzalez et al., 2012), sediment unloading by river erosion (Calais et al., 2010), continental water storage (e.g., Bettinelli et al., 2008; Chanard et al., 2014; Constain, 2016; Fu & Freymueller, 2012), tidal loading (Luttrell & Sandwell, 2010), ice and snow load (e.g., Heki, 2003; Hetzel & Hampel, 2005), and heavy precipitation (Hainzl et al., 2006). Roughly speaking, the removal of overburden can create stress perturbations that may have the potential to trigger earthquakes with reverse kinematics as observed for instance in NW Transverse Ranges (Yerkes et al., 1983) and northward of Lorca city (Gonzalez et al., 2012). Conversely, surface loads such as reservoir impoundment, heavy precipitation, and basin loading may trigger earthquakes with prevailing normal kinematics (e.g., Brothers et al., 2011). These observations suggest the possibility of a link between local stress perturbations and the timing of earthquakes, therefore highlighting a possible modulation of seismicity occurrence (i.e., advancing or delaying future earthquakes) over an active tectonic area. For instance, King et al. (1994) evidenced how an increase of Coulomb stress, related to the 1979 Homestead Valley and 1992 Joshua Tree aftershock distributions, occurred along much of the Landers rupture zone, therefore advancing the Landers earthquake by one to three centuries. The same authors pointed out also that the Landers earthquake, in turn, increased the Coulomb stress at site of the future *M*6.5 Big Bear aftershock and that both earthquakes raised the stress

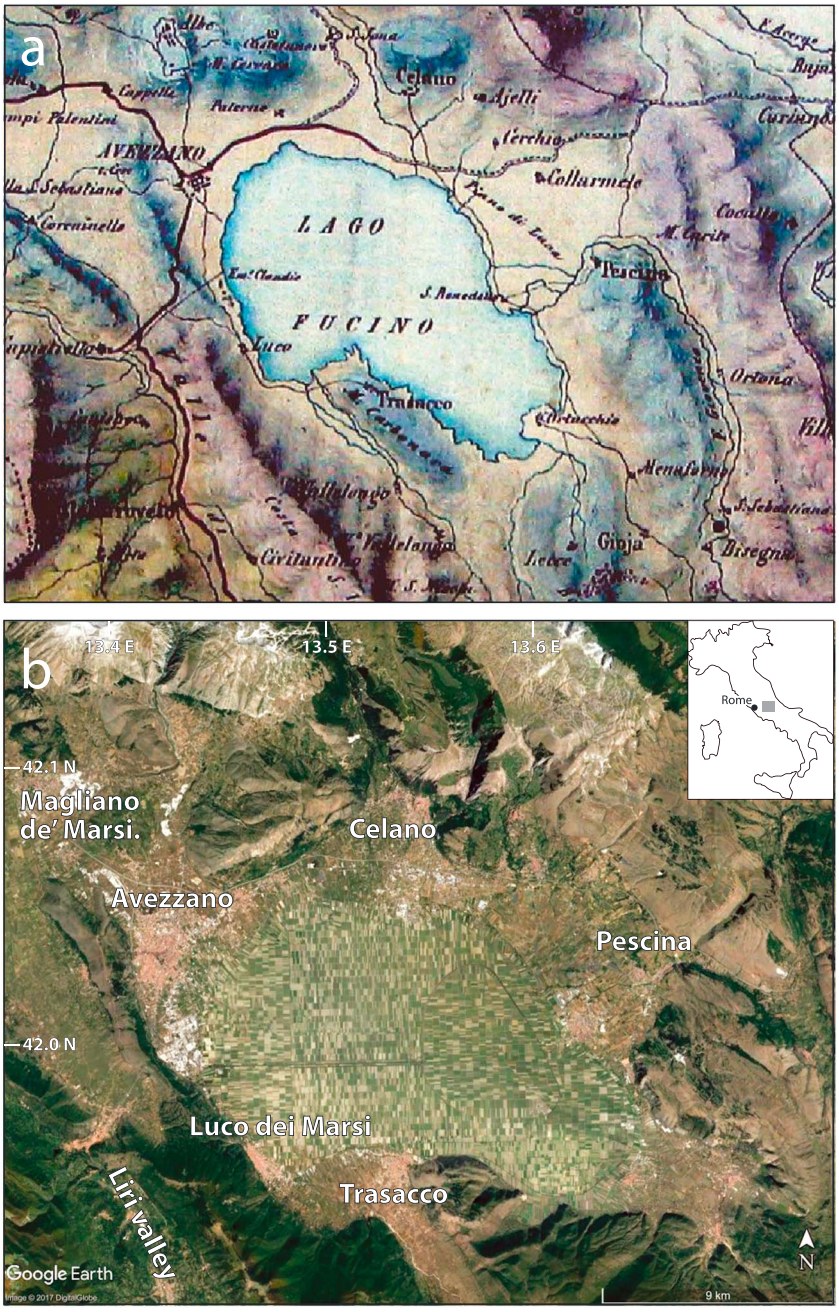

Figure 1. (a) Old map (1854) showing Lake Fucino before modern draining (available at https://www.flickr.com/photos/peetastn/38955575/sizes/z/); and (b) the former Fucino Lake area as seen from satellite imagery (2017).

along the San Bernardino segment of the southern San Andreas fault by 0.2–0.6 MPa, advancing the next large earthquake there by about a decade. Conversely, Toda and Stein (2002) observed that the *M*6.5 Coalinga and *M*6 Nuñez events decreased the Coulomb stress on the Parkfield segment of the San Andreas fault, causing a dropping of surface creep and seismicity rates, therefore leading to a temporal delay of the occurrence of $M \sim 6$ earthquakes along that segment.

Here we explored a possible relationship between the dewatering of the large endorheic lake that formerly occupied the Fucino intermountain basin (Central Italy; Figure 1) and the occurrence of seismicity recorded in the area since the twentieth century and culminated with a *M*7.1 earthquake in 1915 (Cucci & Tertulliani, 2015). With the exception of the *M*5.7 earthquake that occurred in 1904, Table 1 shows that no seismic event

Table 1
List of the Seismic Events That Occurred in the Fucino Area Between 1000 and 1915 (CPTI15 Catalogue, Rovida et al., 2016)

Event's date[a]	Latitude	Longitude	Io	M_w
1-11-1633	42.064	13.601	5	-
19-1-1648	42.064	13.601	4.5	-
April 1742	42.084	13.546	5	4.2 ± 0.5
May 1742	42.084	13.546	5	4.2 ± 0.5
1742	42.084	13.546	5.5	4.4 ± 0.5
1743	42.046	13.454	5.5	4.4 ± 0.5
24-1-1778	42.153	13.534	6.5	4.9 ± 0.5
30-12-1850	42.048	13.514	6.5	4.9 ± 0.5
15-4-1887	41.995	13.482	4.5	3.9 ± 0.5
9-5-1891	41.804	13.486	5	4.4 ± 0.2
29-12-1900	41.744	13.575	4.5	4.1 ± 0.3
24-2-1904	42.097	13.316	8.5	**5.7** ± 0.1
25-2-1904	42.076	13.319	5.5	4.6 ± 0.3
3-3-1904	42.032	13.426	4.5	4.3 ± 0.3
10-3-1904	42.092	13.363	5	4.2 ± 0.5
20-3-1904	42.064	13.342	5.5	4.4 ± 0.5
29-3-1904	42.092	13.363	5.5	4.4 ± 0.5
22-2-1910	42.092	13.363	5	4.2 ± 0.5
3-1-1913	41.868	13.657	5.5	4.5 ± 0.2
14-4-1914	42.022	13.578	5	4.3 ± 0.3
13-1-1915	42.014	13.530	11	**7.1** ± 0.1

Note. The 1633 and 1648 earthquakes (Castenetto & Galadini, 1999) are not quoted in the Catalogue, so their macroseismic magnitude is not computed. Io = epicentral intensity.
[a]Dates in numbers are formatted as day-month-year.

with $M > 4.9$ has been documented in the investigated area since 1000 CE (Common Era; Rovida et al., 2016). Therefore, the occurrence of the 1915 earthquake surprised a largely inadequate building stock, causing a nearly total destruction of many villages within a large area and causing about 30,000 fatalities (Oddone, 1915). Because of the very modest seismic release over the investigated area, a possible influence of the dewatering of the Fucino Lake on the occurrence of the 1915 earthquake has been hypothesized (see Castenetto & Galadini, 1999, and references therein for additional details). Since no quantitative attempts to verify such a hypothesis have been proposed in the scientific literature so far, in this study we performed some numerical simulations to estimate the stress changes induced by (i) the dewatering of the Fucino Lake and by (ii) the *M*5.7 1904 earthquake. We computed the stress changes on a couple of modeled faults selected from the wide spectrum of the ones proposed in literature as the seismogenic source of the Fucino earthquake (see Cucci & Tertulliani, 2015 for an overview).

2. The Fucino Lake

The Fucino plain designates an unusually flat area situated at an average altitude of 650–670 m above sea level (asl) in a broadly mountainous region (Figure 1). The lake that formerly occupied this area until the nineteenth century was a large endorheic basin stretching between the villages of Avezzano to the northwest and Ortucchio to the southeast. At the time of its draining the lake was the largest lake of peninsular Italy, covering a maximum area of ~150 km^2, with an estimated volume of water of ~2.18 km^3 and a rather constant depth of ~20 m. The hydrological regime of the basin was mainly controlled by the activity of karst sinkholes. However, the lack of natural effluents caused a high variability of the lake level in historical times, the ultimate climatic factors controlling such variations being the rainfall and the summer evapotranspiration (Giraudi, 1989). Therefore, although the Fucino has been agriculturally developed for almost 2,000 years, providing fertile soil and a large amount of fish, in the Roman era it suffered repeated severe floods during the rainy season, posing the question of a definitive solution for the mitigation of the flood hazard. To this aim, Emperor Claudius inaugurated an engineering project in 52 CE to drain the excess waters into the deeper Liri Valley to the southeast. A 5-km-long tunnel emerging at a point 8 m below the average shore level was excavated through the rock to keep the lake within its banks, but the too expensive maintenance resulted in its abandonment during the decadence of the Roman Empire (fifth to sixth centuries CE). The Swiss engineer Mayor de Montricher, who was commissioned by landlord Prince Torlonia to permanently dewater the lake, carried out a most ambitious engineering project in the nineteenth century. A 6.3-km-long, 21-m-wide deeper tunnel was begun in 1855, and the lake was completely drained in 1877, after more than 20 years. The new farmland was divided into small parcels and colonized; several small villages located by the former lakeshore rapidly developed, and the old lake became the most important agricultural site of the region.

3. Geological and Seismotectonic Framework

The structure of the Apennines fold-and-thrust belt of Central Italy is mainly due to Neogene compressive tectonics, which produced severe shortening across NW trending, thrust faults. Since Late Pliocene-Early Pleistocene, this belt (and markedly its axis zone) has been affected by NE-SW extension (and/or gravity collapse driven by tectonic uplift during crustal shortening; see, for instance, Doglioni et al., 2015; Patacca et al., 2008). As a consequence of this tectonic phase, repeated normal faulting activity along 10- to 30-km-long, mainly NW trending structures was responsible for the formation of some intermontane basins. The Fucino Plain is one of the largest basins in this region, composed of a 10-km-thick sequence of Upper Triassic-Upper Cretaceous platform dolomites and limestones. The basin is filled by a +1,000-m-thick sequence of Pleistocene and Holocene, low-density lacustrine and fluvial deposits that originate a 15- to 20-mGal local gravimetric minimum in the central part of the structural depression (Patacca et al., 2008). Thin layers of

Middle-Upper Pleistocene volcanic fall products from the Tyrrhenian volcanoes interbed with the continental deposits, whereas terraced Middle-Upper Pleistocene alluvial fans mark the northern border of the basin. The tectonic deepening of the basin was mainly controlled by NW-SE normal faults that border the eastern side of the Plain and still mark the present-day tectonic style and seismicity. In such a contest, these faults currently account for an extension rate of 3.1 ± 0.7 mm/year as inferred by geological observations (e.g., Faure Walker et al., 2012). In addition, geodetic observations (Chiarabba & Palano, 2017; Shen et al., 2015; see supporting information Text S1 and Figure S1 for details on geodetic velocity field and estimated strain-rate pattern) show that such extensional deformation (35 ± 5.4 nanostrain/year) is affecting a ~45-km-wide belt and is occurring along NNE-SSW to NE-SW attitudes.

Although the Fucino basin was characterized by the occurrence of the *M*7.1 1915 earthquake and of another moderate seismic event in 1904 (*M*5.7), the analysis of the seismicity shows that the Fucino area can be considered a low-seismicity region. As a matter of fact, the analysis of the recent instrumental seismicity shows that only small earthquakes, infrequent in time, affect the region. From 1985 to date the National Seismic Network recorded 1,350 events of $0.2 < M < 4.1$ but only 35 events with $M > 3.0$ (ISIDe working group, 2016).

From 1000 CE to 1877 (Rovida et al., 2016), when the dewatering of the lake was completed, no damaging earthquake is on record except two small events (Mercalli-Cancani-Sieberg [MCS] intensity of 6–7) in 1778 and 1850. No earthquake is on record before 1742 (see Figure 3 and Table 1 for a complete view of the seismic history of the region). In addition, recent studies (e.g., Socciarelli, 2016) based on information reported on some original documents (stored in local archives) reported the occurrence of some small unknown earthquakes especially concentrated within the eighteenth century, almost all without information on damage (Table 1). Furthermore, paleoseismological and archeological investigations hypothesized the destruction of the Roman town Alba Fucens as due to a large event (Galadini et al., 2010) originated in 508 CE on the same fault responsible for the 1915 one, while another probable strong event could be dateable during the thirteenth century (Galli et al., 2016).

After the dewatering of the lake, and before 1915, the seismicity of the area persisted to be low and infrequent. The only significant exception was a moderate *M*5.7 earthquake that occurred on 24 February 1904 along the northwestern sector of the Fucino basin causing heavy damage especially in the localities of Rosciolo de Marsi e Magliano de Marsi. The MCS intensity of the event was estimated as 8–9 (Rovida et al., 2016). The damaged area remained limited to some villages near the epicenter, a few kilometers NW of Avezzano. A short tail of aftershocks followed the 1904 event.

On 13 January 1915, one of the largest and most destructive earthquakes in the Italian Peninsula hit the Fucino basin, provoking one of the most severe catastrophes of Italian history. The earthquake ruined many tens of villages, demanding 30,000 victims with 90% of mortality in Avezzano. Damage occurred also in Rome, 80 km westward. The MCS intensity of the event was assessed as 11 (Table 1). The seismic sequence was long and caused further damage in the territory. The occurrence of the 1915 earthquake surprised an utterly inadequate building stock, because of the lack of memory of significant earthquakes (Baratta, 1915; Oddone, 1915).

Analyses of the catalogue completeness for this part of Italy indicate that a completeness threshold is fair in a range between 1600 and 1700 for $M \geq 5.5$ (Albarello et al., 2001). Nevertheless, for historical records the mere statistical representation of seismicity is not stringent if it is not matched with a historiographical approach as well (Stucchi et al., 2004). For what has been mentioned so far, the very low frequency in earthquake occurrence over the investigated region could be most probably explained as a gap in the seismic history of the study area due to a lack of local documentary sources, as in other different parts of Italy (Stucchi & Albini, 2000; Tertulliani et al., 2017). It could reflect also a complex geological strain accumulation history with 3- to 5-kyr-long phase of strain accumulation at slow rate (≤0.5–2 mm/year), followed by a cluster of three to four large earthquakes or earthquake sequences that released most of the strain in less than 1–2 kyr as suggested by Benedetti et al. (2013) and Galli et al. (2016).

4. Seismogenic Sources

Based on different approaches and techniques, a wide spectrum of seismogenic faults have been proposed in the past decades as the source of the 1915 Fucino earthquake (see Cucci & Tertulliani, 2015 for a complete

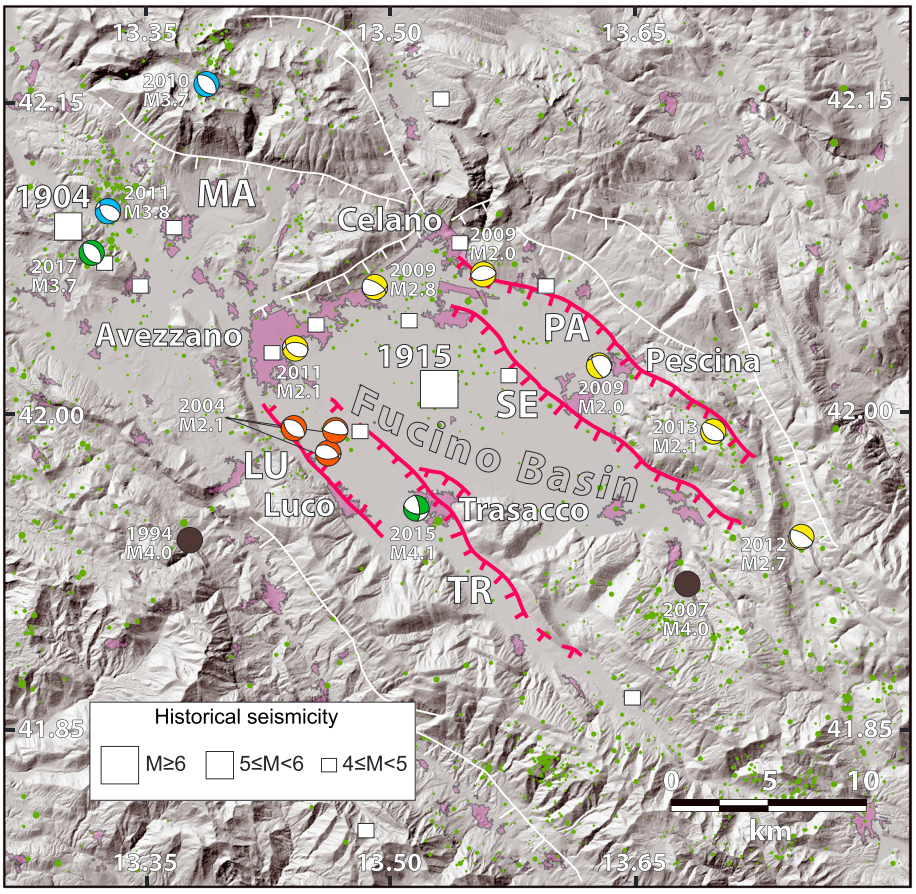

Figure 2. Map of the study area. White squares indicate the historical seismicity from the Catalogue of Italian Earthquakes (Rovida et al., 2016). Green dots indicate $M \leq 3.5$ instrumental seismicity between January 1983 and December 2017 (ISIDe working group (2016). Available focal mechanisms are from http://info.terremoti.ingv.it/tdmt (green), from https://www.slu.edu (blue), from Bagh et al. (2007) (orange), and from Frepoli et al. (2017) (yellow). Purple areas indicate villages and human settlements. Faults modified from Cucci and Tertulliani (2015): Thick red lines mark the segments of the Fucino fault system; thin white lines are other normal faults in the area. LU = Luco fault, MA = Magnola fault, PA = Parasano fault, SE = Serrone fault, TR = Trasacco fault.

review). Among the seismogenic sources proposed, in the following computations we refer to the ones put forward by Galadini and Galli (1999) and by Amoruso et al. (1998).

The former has been proposed on the basis of geological and palaeoseismological observations and is characterized by two 110°–140°N main seismogenic structures (Parasano Fault and Serrone Fault) along with 130°–140°N synthetic (Trasacco Fault) and antithetic (Luco Fault) splay faults located close to the western side of the Fucino basin, in their hanging walls (see Figure 2 and Table 2 for additional details). Such a complex seismogenic structure, characterized by normal faulting features, fits well with the coseismic ruptures mapped in the field by Oddone (1915), with the inversion of geodetic leveling data (Ward & Valensise, 1989), the distribution of macroseismic observations (Rovida et al., 2016), and the hydrological signature of coseismic earthquake strain (Cucci & Tertulliani, 2015).

The latter is given by a simple rectangular source, which is inferred from a joint nonlinear inversion of seismic (*P* wave polarities) and geodetic (elevation changes) data. This source shows a significant left-lateral component (rake of −42°; see Table 2 for details) in addition to normal slip on a NW striking, SW dipping normal fault roughly corresponding to the Serrone Fault (Figure 2).

We consider both selected seismogenic sources well representative of the wide spectrum of the ones proposed as the source of the Fucino earthquake. Moreover, we discarded those sources favoring pure strike-slip or reverse faults (e.g., Basili & Valensise, 1991; Gasparini et al., 1985) because of their

Table 2
Parameters of Seismogenic Sources of the 1915 Earthquake Used as Fault Planes for Computing the Coulomb Stress Changes

Source	Fault ID	Length (km)	Width (km)	Minimum depth (km)	Maximum depth (km)	Strike (deg)	Dip (deg)	Rake (deg)	Slip (m)
Am98		35.0	9.0	2.0	9.4	143	55	−42	1.23
GG99	Parasano Fault	6.9	17.3	0.0	15.0	131	60	−90	1.3
	Serrone Fault	13.3	17.3	0.0	15.0	135	60	−90	0.8
	Trasacco Fault	8.5	17.3	0.0	15.0	137	60	−90	0.9
	Luco Fault	7.7	3.5	0.0	3.0	319	60	−90	0.3

Note. Fault segments belonging to the fault system proposed by Galadini and Galli (1999) are also indicated. Am98 = Amoruso et al. (1998); GG99 = Galadini and Galli (1999).

inconsistency with respect to the extensional feature of the investigated area as evidenced from geological and geodetic observations (Figure S1). Finally, both selected seismogenic sources are considered, in recent literature, as the most likely causative sources for the Fucino earthquake (see Cucci & Tertulliani, 2015, and references therein).

The *M*5.7 1904 seismic event affected a limited number of villages located in the northwestern side of the Fucino plain; based on the earthquake epicenter location, Galadini et al. (1997) suggested the westernmost portion of the Magnola fault (Figure 2) as its causative source. No focal mechanism is available for this event, although Galli et al. (2012) suggested normal faulting kinematics on the basis of the similarity with small-magnitude earthquakes occurring between 2001 and 2004 striking the same area.

5. Numerical Modeling

In order to evaluate the stress changes induced by the dewatering of the Fucino Lake on the 1915 earthquake source, we set up a 3-D numerical poroelastic model. As mentioned above, the computations have been performed on the sources proposed by Galadini and Galli (1999) and by Amoruso et al. (1998). Parameters of both seismogenic sources are summarized in Table 2.

5.1. Mathematical Formulation

In our model, the variations in the lake water level alter the stress conditions on the fault planes by two main physical processes: (i) the static unloading due to the dewatering procedure changes the shear ($\Delta\tau$) and normal stresses ($\Delta\sigma_n$) on the fault plane, and (ii) the dewatering perturbs the pore pressure (Δp) in the rocks below the reservoir due to pore-pressure diffusion. These effects can be expressed in terms of the effective Coulomb stress changes as:

$$\Delta CFF = \Delta\tau + \mu(\Delta\sigma_n + \Delta p) \tag{1}$$

where μ is the friction coefficient. Indeed, because of the presence of fluids in rocks pores, $\Delta\sigma_n$ is effectively reduced by the change in pore pressure Δp. Therefore, estimations of stress field and pore pressure changes need to be jointly computed by solving a coupled hydromechanical model. The flow of groundwater in saturated porous media is described by the governing equations derived from the fundamental principle of mass conservation (continuity equation) and Darcy's law:

$$\begin{aligned} &\frac{\partial(\phi\rho_f)}{\partial t} + \nabla\cdot(\rho_f\mathbf{u}) = 0 \\ &\mathbf{u} = -\frac{\kappa}{\eta}\nabla p \end{aligned} \tag{2}$$

where $\mathbf{u}$ is the flow velocity, k the permeability, η the viscosity, ρ_f the density of the fluid, p the pore pressure, and ϕ the medium porosity. Porosity and fluid density changes in the continuity equation can be related to pore pressure changes. Rice and Cleary (1976), among others, have presented the relationships of porosity and density changes in terms of compression moduli and pore pressure changes. Recasting their results under isothermal condition, equation (2) can be written as:

$$\rho_f S\frac{\partial p}{\partial t} + \rho_f\alpha_B\frac{\partial\varepsilon_V}{\partial t} + \nabla\cdot(\rho_f\mathbf{u}) = 0 \tag{3}$$

with S the storage coefficient, α_B the Biot coefficient, and ε_V the volumetric strain of the rock matrix (Neuzil, 2003). A full description of the fundamental equations of poroelasticity can be found in Detournay and Cheng (1993) and Wang (2000). The second term in equation (3) accounts for the coupling between the deformation of the rock matrix and the pore pressure changes. The strain of the rock matrix is related to its mechanical state. Assuming that the timescale of deformation is slow enough compared to the timescales of elastic waves, the rock is in quasi-static equilibrium, which in terms of the stress tensor $\boldsymbol{\sigma}$ is stated as:

$$\nabla \cdot \boldsymbol{\sigma} = 0 \tag{4}$$

A 3-D finite elements model under the software COMSOL Multiphysics (COMSOL Multiphysics 5.0, 2014) is set up to simultaneously solve for (i) the Darcy flow equation (equation (2)), (ii) the mass conservation equation (equation (3)), and (iii) the elastostatic equilibrium (equation (4)), thus allowing for a full coupling between the fluid flow and the mechanical stress state. Details of model setup are provided in the supporting information (Text S2).

5.2. Computational Domain, Model Parameter, and Results

The computational domain extends 100 × 100 × 20 km around the Fucino Lake and takes into account the real topography derived from the Shuttle Radar Topography Mission data. The lake surface is delimited by the isoline at 670 m asl (according to the location of the shoreline altimetrical monuments; see Loperfido, 1919, for details). The mechanical and hydrological parameters of the model domain have been deduced from seismic tomography (Chiaraluce et al., 2009) and rock laboratory analysis (Agosta et al., 2007). In particular, the average 1-D P wave velocity model (Chiaraluce et al., 2009) revealed relatively high V_p values which varies almost linearly from 5.3 to 6.8 km/s going from shallow to 20-km depth. The average V_p/V_s ratio is about 1.83. The density of the medium increases from 2,500 to 2,700 kg/m^3 going from the top to the bottom of the domain. On the basis of the seismic velocities and densities, the Young's modulus and the Poisson's ratio have been estimated according to the following relationships (Kearey & Brooks, 1991):

$$\begin{aligned} E &= 2\rho_r V_s^2(1+\nu) \\ \nu &= \left[\left(V_p/V_s\right)^2 - 2\right] / \left[2\left(V_p/V_s\right)^2 - 2\right] \end{aligned} \tag{5}$$

which provide an average Poisson ratio of 0.28. The values of Young's modulus are corrected by a factor of 0.7 to account for the difference between the static and dynamic modulus and increase with depth from 35 to 70 GPa. These values are also in agreement with the ones obtained from laboratory tests on rock samples collected along basin-bounding normal faults in the southeast side of the Fucino basin (Agosta et al., 2007). Petrophysical analyses on the carbonate rocks report on very low values of permeability and porosity of the host rock (Agosta et al., 2007). Roughly speaking, rock permeability is a quantity that may vary by several (more than 5) orders of magnitude, even for a single rock type. Typical values for crustal rocks permeability range from 10^{-19} to 10^{-14} m^2, with an average value of 10^{-18} m^2. Permeability is sensitive to overburden pressure also, resulting in a general decrease with respect to depth increase. In such a regard, Ingebritsen and Manning (1999, 2010) suggested that the mean permeability of tectonically active continental crust decreases with depth following a quasi-exponential decay rate of $\log(k) \approx -14–3.2\log(z)$, where k is in square meters and z is the depth in kilometers and downward positive. Because of the lack of detailed constraints on crustal rock permeability values in the investigated domain, we performed some numerical simulations in order to analyze the effect of permeability on the results. Particularly, we investigate three homogeneous permeability models (hereinafter *M17*, *M18*, and *M19*; see Table S1 in the supporting information), by ranging the rock permeability within the 10^{-17}–10^{-19} m^2 interval, and a depth-dependent permeability model (hereinafter *Mdd*) according to the above studies. In all models we fixed the porosity of the host rock to the value of 0.01.

The Biot coefficient α_B, which relates the volume of fluid expelled or introduced in a porous material element to the volumetric change of the same element (equation (3)), depends on the properties of the porous matrix and is bounded to $\phi < \alpha_B \leq 1$. To allow for a maximum coupling between the pore volume change and the volumetric strain rate (equation (3)), α_B was set equal to 1, which also represents a reasonably high value found in carbonate rocks. The storage coefficient S depends on basic material properties, as porosity and

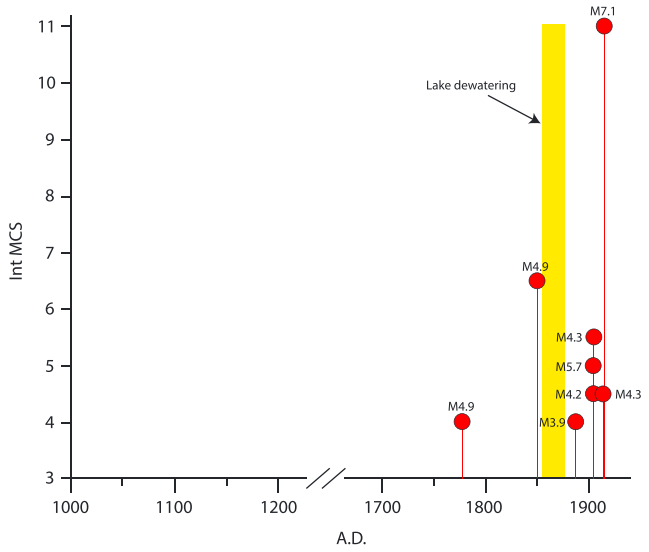

Figure 3. Felt intensities between 1000 and 1915 in the town of Avezzano (the most important urban center in the Fucino area; see Figure 1) for earthquakes located within 25 km from the town. MCS intensities and equivalent magnitudes are from Rovida et al. (2016). The yellow shaded rectangle indicates the period of the dewatering of the lake (1855–1877). MCS = Mercalli-Cancani-Sieberg.

the compressibility of fluid and solid matrix. Using a water compressibility of $4.5 \cdot 10^{-10}$ Pa^{-1} and the estimated elastic rock compressibility, the storage coefficient S values range from $2.5 \cdot 10^{-11}$ to $4.9 \cdot 10^{-11}$ Pa^{-1}.

Pore pressure and stress field components have been computed under the action, over the time, of the depressurization exerted by the dewatering of the Fucino Lake. Stress-free boundary conditions have been assigned on the ground surface except on the assumed lake surface, where a pressure unloading is applied according to

$$p(x,y,t) = -\rho_f g h(x,y,t) \quad (6)$$

where $h(x,y,t)$ is the water level change, whose spatial distribution is computed as the difference between the isosurface at 670 m asl and the actual topography. As unloading time history, a continuous linear increase is simulated over the 22-year-long dewatering process (hereinafter T1), that started in 1855 and ended in 1877 (Figure 3).

For each of the above mentioned models, we estimated also the height variations (as resulting at the end of the simulation time in 1915), on the lake surface and on the 18 altimetrical monuments (Figures S2 and S3), located along the shoreline within a few centimeters of the free level of the lake in 1862, during the early stage of lake drainage (Loperfido, 1919). Achieved results show a similar pattern, with exponentially increasing height variations over T1, followed by very small decreasing height variations during the 1877–1915 period (hereinafter T2). Results obtained for models *M17*, *M18*, and *M19* have a very similar pattern (differences are lesser than 1% on the maximum height change, i.e., 1.19 cm at p09 monument; Figures S2 and S3), while results coming from model *Mdd* are characterized by slightly lesser height variations (lesser than ~7% on average) during T1 and slightly marked decreasing height variations during T2, especially on altimetrical monuments close to the deepest sector of the lake. Roughly speaking, the height variations estimated during T1 are mainly produced by the static unloading contribute due to the dewatering process, while height variations estimated during T2 reflect the poroelastic contribution of pore pressure diffusion. In the model *Mdd*, where the surficial pressure diffusion timescale is faster due to the higher permeability value in the shallow crust (10^{-14} m^2), a compaction effect is noticeable soon after the dewatering procedure. Moreover, it must be noted that all these modeled variations are very small (lesser than uncertainties associated to observed coseismic variations Ward & Valensise, 1989). Based on all these results and considerations, in the following we refer to Coulomb stress changes achieved from *M18* model (Figure 4). We selected this model, since the adopted rock permeability value is based on the one estimated by petrophysical analyses in Agosta et al. (2007).

The effective Coulomb stress changes resulting at the end of the simulation time (1915) are computed by projecting the stress tensor onto the fault surfaces (Figure 4). Estimated Coulomb stress values range from −42 to 17 kPa interval with predominantly negative stress changes on all the modeled seismogenic sources (a small lobe characterized by positive values up to 17 kPa can be observed along a shallow and limited portion of the Amoruso et al., 1998 source; Figure 4b).

To better examine the stress change distributions at depth, some stress changes maps (Figures 4c and 4d) have been also computed by resolving the stress tensor onto the representative fault planes (Table 2). For the Galadini and Galli (1999) seismic source an average fault plane (strike 135°, dip 60°, and rake −90°) has been assumed. The Coulomb stress changes were computed on a horizontal surface at 4,600 m below sea level depth for the Galadini and Galli (1999) source and at 5,000 m below sea level for the Amoruso et al. (1998) source, corresponding to the depths of the maximum changes, respectively. Both stress patterns show that the main negative variations are confined below the lake surface. Negligible positive changes (less than 10 kPa) are achieved on a NE-SW direction.

We have also investigated a possible promoting effect of the 1904 seismic event on the 1915 event. Pore pressure diffusion over distances and widths of about 2.5 and 0.5 fault lengths is negligible

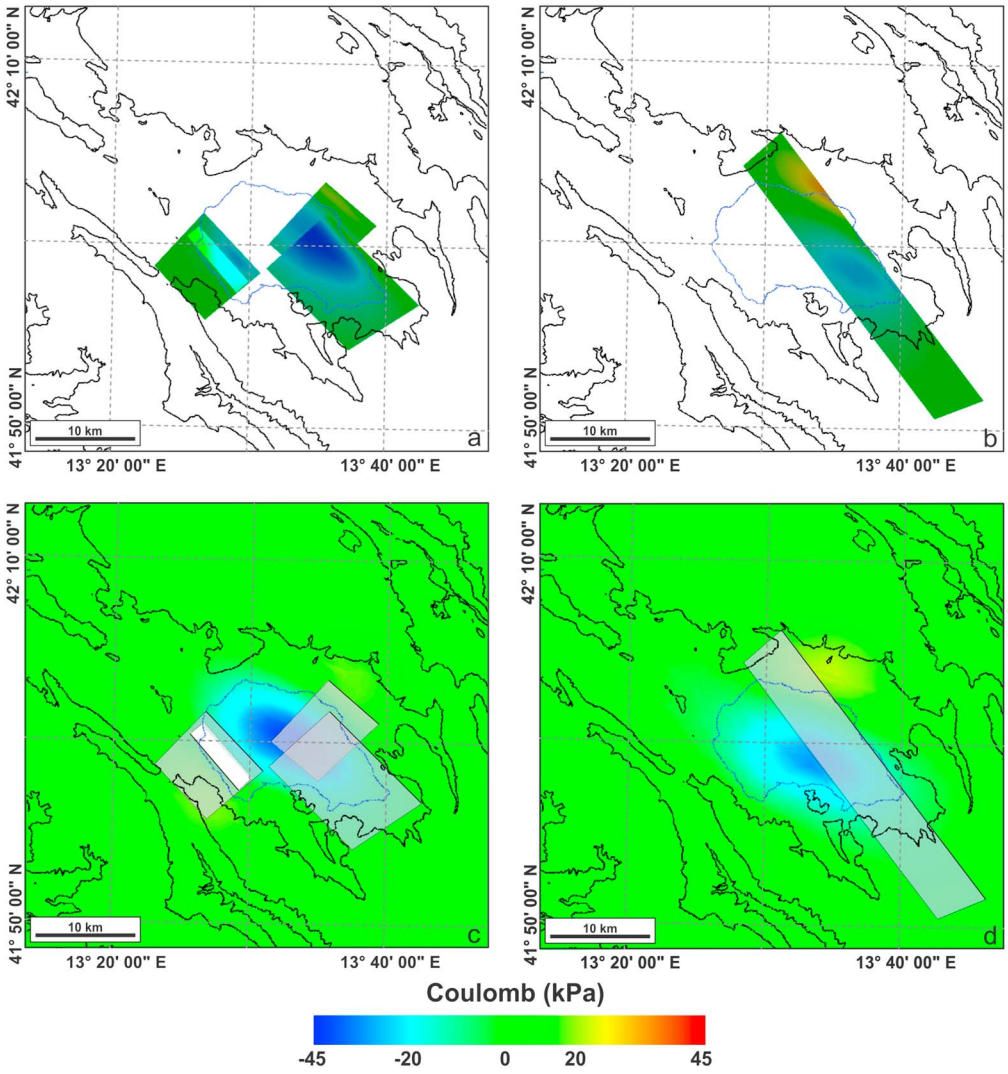

Figure 4. Poroelastic Coulomb stress changes induced by the lake dewatering process resolved onto the seismogenic sources proposed by (a) Galadini and Galli (1999) and (b) Amoruso et al. (1998). Map views of the stress changes projected onto representative fault planes for (c) Galadini and Galli (1999; strike 135°, dip 60°, and rake −90°; Table 2) and (d) Amoruso et al. (1998) seismogenic sources (strike 143°, dip 55°, and rake −42°; Table 2). The stress patterns have been imaged at depth of (c) 4,600 m below sea level and (d) 5,000 m below sea level, where the stress changes reach the maximum amplitude along the fault planes.

(Piombo et al., 2005). The relevant distance over which these effects matter is the hydraulic diffusion length. Therefore, we neglect the effect of pore pressure diffusion to compute the stress changes induced by the 1904 seismic event on the distant faults considered here. Under elastic conditions and following the approach described in Currenti et al. (2008), we computed the stress changes (*M04E*) induced by the rupture of the 1904 fault, whose seismic source parameters (Table 3) are estimated using the Boxer method (see Gasperini et al., 2010, for details). The magnitude M is related to the seismic moment M_o (in Newton-meter) and the seismic source parameters by the following relations (Hough, 1996; Kanamori & Anderson, 1975):

$$\begin{aligned} \log_{10}(M_o) &= 1.5M + 9.1 \\ M_o &= \mu AD \end{aligned} \tag{7}$$

where μ is the shear modulus of the crust (in pascals), A is the area of the fault rupture (in square meters), and D is the average displacement over the rupture surface (in meters). A displacement of 41 cm over an area of

Table 3
Parameters of the 1904 Earthquake Source[a], Used as Input for Modeling the Coulomb Stress Changes on the Selected Sources Related to the 1915 Earthquake[b]

Parameters	Values
Estimated magnitude	5.71
Fault length (km)	8.5
Fault width (km)	6.6
Fault strike (degree)	N92.4
Fault dip (degree)	60
Epicenter (Long., Lat.)	42.0968, 13.3162

[a]Estimated by using the Boxer code; Gasperini et al., 2010). [b]Table 2.

56.1 km^2 is estimated from a magnitude value of 5.71 and using an average rigidity modulus of 20 GPa. The 1904 fault is southward dipping with a dip angle of 60°. Resulting Coulomb stress changes, projected onto the fault surfaces, are reported in Figure 5. Estimated Coulomb stress values range from −1 to 10 kPa interval with highest values observed on a very limited portion of the northern sectors of the Trasacco and Luco faults (Figure 5a). These findings are further evidenced by taking into account the Coulomb stress changes distribution at depth, resolved for representative fault planes (see Figure S4 in the supporting information). These low values are due to the (i) moderate magnitude of the 1904 earthquake and (ii) the distance of the 1915 seismogenetic sources with respect to the 1904 one.

6. Discussion

The 1915 earthquake hit a region characterized during the past 1,000 years by a very modest seismic release; therefore, we investigated whether the occurrence of such earthquake corresponds to predictions from Coulomb stress changes due to local sources of stress perturbation. To this aim we performed two numerical simulations in order to estimate the stress changes induced by (i) the dewatering of the Fucino Lake and by (ii) the *M*5.7 1904 earthquake. As mentioned above, the stress changes have been computed on a couple of modeled faults, selected among the wide spectrum proposed in literature as the seismogenic source of the Fucino earthquake.

Poroelastic Coulomb stress changes (*M18* model) as resulting at the end of the simulation time (1915) are computed by projecting the stress tensor onto the fault surfaces of both selected seismogenic sources (Figure 4). Regarding the Galadini and Galli (1999) sources, computed stress changes are mainly negative with a maximum value of about −42 kPa on the Parasano Fault and Serrone Fault whose projections in depth are located below the dewatered region (Figure 4a). Coulomb stress changes with positive values up to 9 kPa can be observed on the northern edge of the Luco Fault, at a very shallow depth. Negative stress changes of about −20 kPa and −10 kPa have been computed on the Trasacco Fault and on the Luco Fault, respectively. Similar results (~ −27 kPa) have been achieved for the Amoruso et al. (1998) seismogenic source (Figure 4b),

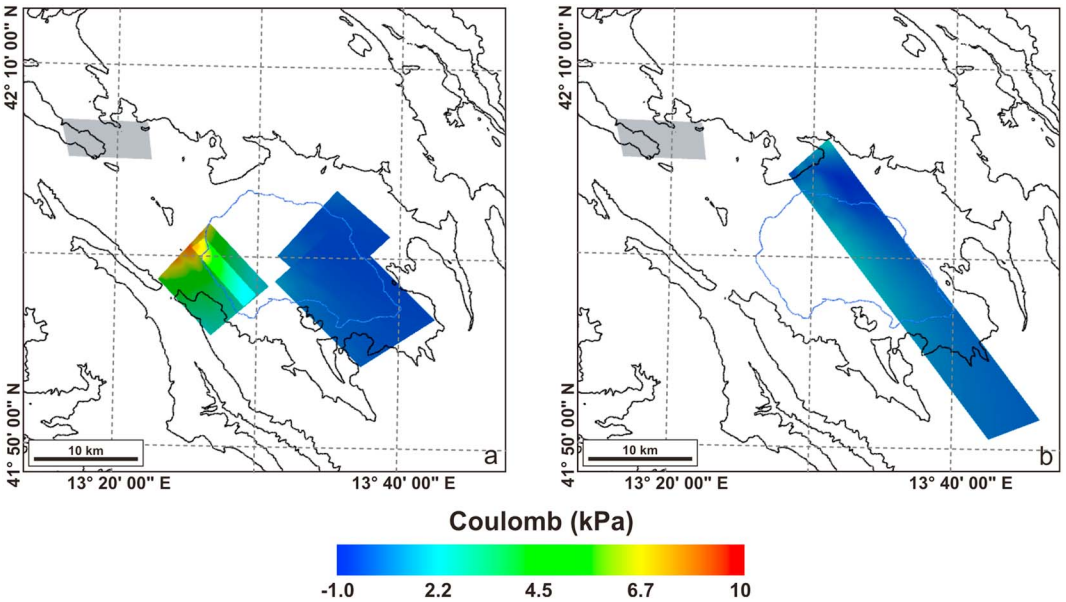

Figure 5. Stress change induced by the 1904 earthquake (the light gray rectangle represents the causative source of the event; see Table 3 for details on parameters) resolved onto the seismogenic sources proposed by (a) Galadini and Galli (1999) and (b) Amoruso et al. (1998).

with a small lobe characterized by positive values up to 17 kPa along a shallow and limited portion of its northern segment. We consider such a lobe of positive Coulomb stress changes not able to trigger seismic events because of its limited areal extension. All these results highlight how the primary effect of the dewatering process on both selected seismogenic sources is a decrease of stresses along the fault planes. These results imply that dip- and oblique-slip along the fault planes is hampered. Roughly speaking, positive Coulomb stress changes bring seismogenic faults closer to failure, while negative values move the fault farther from failure, hence delaying the next earthquake (Stein, 1999). These considerations suggest that the lake dewatering may have slightly unloaded the fault in a preexisting critical state and may have delayed the stronger seismic rupture in 1915.

However, all these results and considerations are based on a poroelastic rheology. Indeed, viscoelastic relaxation of the lower crust may influence both deformation and stress field evolution. In order to evaluate possible viscoelastic time dependence contributions to the deformation and stress fields, we performed some additional simulations by adopting a more composite model with a stack of horizontal layers with different rheology and extending the computational domain down to a depth of 30 km, that is, the average Moho depth below the investigated region (Piana Agostinetti & Amato, 2009). More in detail, we explored a three-layer domain model (*M3L*; see Table S1 in the supporting information for additional details) defined as (i) an upper layer (2 km below the sea level and taking into account the real topography) with poroelastic assumption, (ii) an intermediate layer, located in the 2- to 15-km depth interval, with elastic rheology, and (iii) a lower layer (i.e., lower crust), below a depth of 15 km, with a standard linear solid (SLS) viscoelastic rheology using an average viscosity of 10^{18} Pa·s. The depth of 2 km represents the typical depth where the coseismic slip on many normal faults start decreasing according to geodetic-based models for large Apennines earthquakes (e.g., Cheloni et al., 2017 and references therein). Moreover, the depth of ~15 km represents the lower edge of the seismogenetic layer as estimated by the depth distribution of instrumental seismicity (e.g., Chiarabba & De Gori, 2015). In addition, we also investigated a two-layer domain model (*M2L*; Table S1) defined as (i) an upper layer (15 km below the sea level and taking into account the real topography) with poroelastic assumption and (ii) a lower layer (i.e., lower crust), below a depth of 15 km, with SLS viscoelastic rheology (assumed viscosity of 10^{18} Pa·s).

For both models we estimated the height variations at the altimetrical monuments bordering the lake shoreline over T1 and T2 time intervals (Figure S5). The patterns of deformation over the time are similar to the one already obtained for models *M17*, *M18*, and *M19*, with positive height variations during T1 (height change of 1.86 and 1.58 cm at p09 monument for *M3L* and *M2L*, respectively) and no significant deformation during T2. Such results well highlight how the temporal evolution of crustal surface deformation is sensitive to the rate of the dewatering process and poorly sensitive to lower crustal flow. These results are justified by the low deloading water volume (~2.18 km^3) and the small spatial footprint of the lake surface.

We estimated also the temporal evolution of Coulomb stress changes at the center of the Amoruso et al. (1998) source and on the Serrone fault of Galadini and Galli (1999) source (Figure S5); both selected points have been characterized by the (absolute) highest stress change values as resulting from *M18* model (Figure 4). Modeled values (e.g., −40 kPa and −44.5 kPa, for *M2L* and *M3L*, respectively) are very close to those obtained for *M18* model (−42 kPa), suggesting again a negligible contribute of the lower crustal flow to the surface deformation as well as to the stress changes along fault planes (see Figure S6 for additional details). Coulomb stress changes related to the *M*5.7 1904 earthquake (*M04E*) are reported in Figure 5. In this case, we observed positive stress changes on both the Galadini and Galli (1999) and on the Amoruso et al. (1998) seismogenic sources. Regarding the Galadini and Galli (1999) seismogenic sources (Figure 5a), we observed Coulomb stress values lesser than 10 kPa and mainly concentrated on a limited portion of the northern sectors of the Trasacco and Luco faults. Coulomb stress values are very small (~ −0.3 kPa) for both Parasano and Serrone faults. Regarding the Amoruso et al. (1998) seismogenic source (Figure 5b), positive stress changes with values up to 1 kPa can be observed. Similar Coulomb stress patterns have been obtained by taking into account the *M2L* domain model (Figure S7), which refers to a lower layer with a SLS viscoelastic rheology (see Table S1 for additional details). Although the extent and size of the stress perturbation required to trigger an earthquake is still debated (Avouac, 2012), it is widely accepted that seismicity within a rock volume close to the critical state of failure can be triggered by Coulomb stress changes larger than 10 kPa (see, for instance, Stein, 1999). Therefore, we believe that our computed stress changes related to the *M*5.7 1904 earthquake should not be relevant for influencing the 1915 earthquake occurrence.

We performed an additional computation, by simply summing the Coulomb stress changes resulting from the lake dewatering (*M18*) and the 1904 earthquake (*M04E*). The 1904 seismogenic source being quite distant from the faults here considered and the dewatering effect being restricted mainly below the lake surface, we implicitly assumed that coupled poroelastic (un-)loading effects in the crust are negligible. Such a final computation, reported in Figure S8 in the supporting information, shows results quite similar to those computed by taking into account the dewatering process alone (*M18*), because of the low stress perturbations due to the 1904 earthquake. This aspect clearly suggests that the dewatering process represents the main perturbation factor of the stress state of the investigated area, before the 1915 earthquake.

Results achieved in this study are clear evidence that the human-related dewatering of the Fucino Lake did not promote the *M*7.1 1915 earthquake while lending credit to a possible delay of earthquake occurrence. Assuming that our poroelastic model provides a complete description of the process, the 1915 earthquake would be delayed by the maximum estimated stress change (42 kPa) divided by the background stressing rate associated with the tectonic strain accumulation (26 kPa/year, considering a strain rate of 35 nanostrain/year as estimated by geodetic data and a Young's modulus of 70 GPa) or ~1.71 years (delay times of ~1.63 and ~1.82 can be estimated from our *M2L* and *M3L* models, respectively). Such a value is extremely small in comparison to the earthquake recurrence interval of 0.5 ± 0.3 kyrs as estimated for the Fucino area by geological and paleoseismological constraints on Late Pleistocene-Holocene fault surface slips (e.g., Benedetti et al., 2013; Galli et al., 2016).

These results definitely set forth that the lake dewatering process might have led only to small temporal modulation of seismicity occurrence in nearby areas, therefore not significantly affecting the seismic cycle of the main faults cutting the Fucino basin.

7. Conclusive Remarks

Results presented and discussed in this study can be summarized as follows:

1. Poroelastic Coulomb stress changes are mainly negative (up to −42 kPa) along both selected seismogenetic sources. Coulomb stress changes estimated from models with a stack of horizontal layers with different rheology show values very close to those obtained from the poroelastic ones, therefore suggesting a negligible contribution of the lower crustal flow to the surface deformation as well as to the stress changes along fault planes.
2. Coulomb stress changes related to the *M*5.7 1904 earthquake range from −1 to 10 kPa interval with highest values observed on a very limited portion of the northern sectors of the Trasacco and Luco faults. Similar Coulomb stress patterns have been obtained by taking into account viscoelastic models also. We suggest that such values did not significantly influence the occurrence of the 1915 event. These considerations suggest that the dewatering process represents the main perturbation factor of the state of stress of the investigated area, before the 1915 earthquake.
3. The human-related dewatering of the Fucino Lake did not promote the *M*7.1 1915 earthquake.

Acknowledgments
We thank the Editor John Geissman, the Associate Editor Mustapha Meghraoui, and three anonymous reviewers for helpful and constructive comments and suggestions. We benefited from a fruitful discussion with Claudio Chiarabba and Luigi Improta who encouraged us to carry out this study. All data used in this paper are reported in the text and in the supporting information.

References

Agosta, F., Prasad, M., & Aydin, A. (2007). Physical properties of carbonate fault rocks, fucino basin (Central Italy): Implications for fault seal in platform carbonates. *Geofluids*, *7*(1), 19–32. https://doi.org/10.1111/j.1468-8123.2006.00158.x

Albarello, D., Camassi, R., & Rebez, A. (2001). Detection of space and time heterogeneity in the completeness of a seismic catalog by a statistical approach: An application to the Italian area. *Bulletin of the Seismological Society of America*, *91*, 1694–1703. https://doi.org/10.1785/0120000058

Amoruso, A., Crescentini, L., & Scarpa, R. (1998). Inversion of source parameters from near- and far-field observations: An application to the 1915 Fucino earthquakes, central Apennines, Italy. *Journal of Geophysical Research*, *103*, 29,989–29,999. https://doi.org/10.1029/98JB02849

Amos, C. B., Audet, P., Hammond, W. C., Burgmann, R., Johanson, I. A., & Blewitt, G. (2014). Uplift and seismicity driven by groundwater depletion in Central California. *Nature*, *509*, 483–486. https://doi.org/10.1038/nature13275

Avouac, J.-P. (2012). Human-induced shaking. *Nature Geoscience*, *5*(11), 763–764.

Bagh, S., Chiaraluce, L., De Gori, P., Moretti, M., Govoni, A., Chiarabba, C., et al. (2007). Background seismicity in the central Apennines of Italy: The Abruzzo region case study. *Tectonophysics*, *444*, 80–92. https://doi.org/10.1016/j.tecto.2007.08.009

Baratta, M. (1915). Le condizioni sismiche della regione marsicana [in Italian]. *La Geografia*, *3*, 106–111.

Basili, A., & Valensise, G. (1991). Contributo alla caratterizzazione della sismicità dell'area marsicano-fucense. In E. Boschi & M. Dragoni (Eds.), *Aree Sismogenetiche e Rischio Sismico in Italia* [in Italian] (pp. 197–214). Erice (TP): Istituto Nazionale Di Geofisica.

Benedetti, L., Manighetti, I., Gaudemer, Y., Finkel, R., Malavieille, J., Pou, K., et al. (2013). Earthquake synchrony and clustering on Fucino faults (Central Italy) as revealed from in situ 36Cl exposure dating. *Journal of Geophysical Research: Solid Earth*, *118*, 4948–4974. https://doi.org/10.1002/jgrb.50299

Bettinelli, P., Avouac, J.-P., Flouzat, M., Bollinger, L., Ramillien, G., Rajaure, S., & Sapkota, S. (2008). Seasonal variations of seismicity and geodetic strain in the Himalaya induced by surface hydrology. *Earth and Planetary Science Letters*, *266*, 332–344. https://doi.org/10.1016/j.epsl.2007.11.021

Brothers, D., Kilb, D., Luttrell, K., Driscoll, N., & Kent, G. (2011). Loading of the San Andreas fault by flood induced rupture of faults beneath the Salton Sea. *Nature Geoscience*, *4*, 486–492. https://doi.org/10.1038/ngeo1184

Calais, E., Freed, A. M., Van Arsdale, R., & Stein, S. (2010). Triggering of New Madrid seismicity by late Pleistocene erosion. *Nature*, *466*, 608–611. https://doi.org/10.1038/nature09258

Castenetto, S., & Galadini, F. (Eds) (1999). *13 Gennaio 1915 Il Terremoto nella Marsica*. Roma: Istituto Poligrafico e Zecca dello Stato.

Chanard, K., Avouac, J. P., Ramillien, G., & Genrich, J. (2014). Modeling deformation induced by seasional variations of continental water in the Himalaya region: Sensitivity of Earth elastic structure. *Journal of Geophysical Research: Solid Earth*, *119*, 5097–5113. https://doi.org/10.1002/2013JB010451

Cheloni, D., de Novellis, V., Albano, M., Antonioli, A., Anzidei, M., Atzori, S., et al. (2017). Geodetic model of the 2016 Central Italy earthquake sequence inferred from InSAR and GPS data. *Geophysical Research Letters*, *44*, 6778–6787. https://doi.org/10.1002/2017GL073580

Chiarabba, C., & De Gori, P. (2015). The seismogenic thickness in Italy: Constraints on potential magnitude and seismic hazard. *Terra Nova*, *28*, 402–408. https://doi.org/10.1111/ter.12233

Chiarabba, C., & Palano, M. (2017). Progressive migration of slab break-off along the southern Tyrrhenian plate boundary: Constraints for the present day kinematics. *Journal of Geodynamics*, *105*, 51–61. https://doi.org/10.1016/j.jog.2017.01.006

Chiaraluce, L., Valoroso, L., Anselmi, M., Bagh, S., & Chiarabba, C. (2009). A decade of passive seismic monitoring experiments with local networks in four Italian regions. *Tectonophysics*, *476*(1–2), 85–98. https://doi.org/10.1016/j.tecto.2009.02.013

COMSOL Multiphysics 5.0 (2014). Comsol Ab, 1356 pp, Stockholm, Sweden.

Constain, J. K. (2016). Groundwater recharge as the trigger of naturally occurring intraplate earthquakes. *Geological Society, London, Special Publications*, *432*, 91–118. https://doi.org/10.1144/SP432.9

Cucci, L., & Tertulliani, A. (2015). The hydrological signature of a seismogenic source: Coseismic hydrological changes in response to the 1915 Fucino (Central Italy) earthquake. *Geophysical Journal International*, *200*, 1374–1388. https://doi.org/10.1093/gji/ggu448

Currenti, G., Del Negro, C., Ganci, G., & Scandura, D. (2008). 3D numerical deformation model of the intrusive event forerunning the 2001 Etna eruption. *Physics of the Earth and Planetary Interiors*, *168*, 88–96. https://doi.org/10.1016/j.pepi.2008.05.004

Detournay, E., & Cheng, A. H. D. (1993). Plane-strain analysis of a stationary hydraulic fracture in a poroelastic medium. *International Journal of Solids and Structures*, *27*(13), 1645–1662. https://doi.org/10.1016/0020-7683(91)90067-P

Doglioni, C., Carminati, E., Petricca, P., & Riguzzi, F. (2015). Normal fault earthquakes or graviquakes. *Scientific Reports*, *5*, 1–12. https://doi.org/10.1038/srep12110

Faure Walker, J. P., Roberts, G. P., Cowie, P. A., Papanikolaou, I., Michetti, A. M., Sammonds, P., et al. (2012). Relationship between topography, rates of extension and mantle dynamics in the actively-extending Italian Apennines. *Earth and Planetary Science Letters*, *325-326*, 76–84. https://doi.org/10.1016/j.epsl.2012.01.028

Frepoli, A., Cimini, G. B., De Gori, P., De Luca, G., Marchetti, A., Monna, S., et al. (2017). Seismic sequences and swarms in the Latium-Abruzzo-Molise Apennines (Central Italy): New observations and analysis from a dense monitoring of the recent activity. *Tectonophysics*, *712-713*, 312–329. https://doi.org/10.1016/j.tecto.2017.05.026

Fu, Y., & Freymueller, J. T. (2012). Seasonal and long-term vertical deformation in the Nepal Himalaya constrained by GPS and GRACE measurements. *Journal of Geophysical Research*, *117*, B03407. https://doi.org/10.1029/2011JB008925

Galadini, F., Ceccaroni, E., & Falcucci, E. (2010). Archaeoseismological evidence of a disruptive late antique earthquake at Alba Fucens (Central Italy). *Bollettino di Geofisica Teorica ed Applicata*, *51*, 143–161.

Galadini, F., & Galli, P. (1999). The Holocene paleoearthquakes on the 1915 Avezzano earthquake faults (Central Italy): Implications for active tectonics in Central Italy. *Tectonophysics*, *308*, 143–170. https://doi.org/10.1016/S0040-1951(99)00091-8

Galadini, F., Galli, P., & Giraudi, C. (1997). Paleosismologia della Piana del Fucino (Italia Centrale) [in italian]. *Il Quaternario*, *10*, 27–64.

Galli, P., Giaccio, B., Messina, P., & Peronace, E. (2016). Three magnitude 7 earthquakes on a single fault in Central Italy in 1400 years, evidenced by new palaeoseismic results. *Terra Nova*, *28*, 146–154. https://doi.org/10.1111/ter.12202

Galli, P., Messina, P., Giaccio, B., Peronace, E., & Quadrio, B. (2012). Early Pleistocene to Late Holocene activity of the Magnola fault (Fucino fault system, Central Italy). *Bollettino di Geofisica Teorica ed Applicata*, *53*, 435–458.

Gasparini, C., Iannaccone, G., & Scarpa, R. (1985). Fault-plane solutions and seismicity of the Italian peninsula. *Tectonophysics*, *117*, 59–78. https://doi.org/10.1016/0040-1951(85)90236-7

Gasperini, P., Vannucci, G., Tripone, D., & Boschi, E. (2010). The location and sizing of historical earthquakes using the attenuation of macroseismic intensity with distance. *Bulletin of the Seismological Society of America*, *100*, 2035–2066. https://doi.org/10.1785/0120090330

Giraudi, C. (1989). Lake levels and climate for the last 30,000 years in the fucino area (Abruzzo-Central Italy). A review. *Palaeogeography Palaeoclimatology Palaeoecology*, *70*, 249–260. https://doi.org/10.1016/0031-0182(89)90094-1

Gonzalez, P., Tiampo, K., Palano, M., Cannavo, F., & Fernández, J. (2012). The 2011 Lorca earthquake slip distribution controlled by groundwater crustal unloading. *Nature Geoscience*, *5*, 821–825. https://doi.org/10.1038/ngeo1610

Gupta, H. (2002). A review of recent studies of triggered earthquakes by artificial water reservoirs with special emphasis on earthquakes in Koyna, India. *Earth-Science Reviews*, *58*, 279–310. https://doi.org/10.1016/S0012-8252(02)00063-6

Hainzl, S., Kraft, T., Wassermann, J., Igel, H., & Schmedes, E. (2006). Evidence for rainfall-triggered earthquake activity. *Geophysical Research Letters*, *33*, L19303. https://doi.org/10.1029/2006GL027642

Heki, K. (2003). Snow load and seasonal variation of earthquake occurrence in Japan. *Earth and Planetary Science Letters*, *207*, 159–164. https://doi.org/10.1016/S0012-821X(02)01148-2

Hetzel, R., & Hampel, A. (2005). Slip rate variations on normal faults during glacial–interglacial changes in surface loads. *Nature*, *435*, 81–84. https://doi.org/10.1038/nature03562

Hough, S. E. (1996). Observational constraints on earthquake source scaling: Understanding the limits in resolution. *Tectonophysics*, *261*, 83–95. https://doi.org/10.1016/0040-1951(96)00058-3

Hua, W., Fu, H., Chen, Z., Zheng, S., & Yan, C. (2015). Reservoir-induced seismicity in high seismicity region-a case study of the Xiaowan reservoir in Yunnan province, China. *Journal of Seismology*, *19*, 567–584. https://doi.org/10.1007/s10950-015-9482-3

Ingebritsen, S. E., & Manning, C. E. (1999). Geological implications of a permeability-depth curve for the continental crust. *Geology*, *27*, 1107–1110. https://doi.org/10.1130/0091-7613(1999)027%3C1107:GIOAPD%3E2.3.CO;2

Ingebritsen, S. E., & Manning, C. E. (2010). Permeability of the continental crust: Dynamic variations inferred fromseismicity and metamorphism. *Geofluids*, *10*, 193–205. https://doi.org/10.1111/j.1468-8123.2010.00278.x

ISIDe working group (2016). Version 1.0. https://doi.org/10.13127/ISIDe

Kanamori, H., & Anderson, D. L. (1975). Theoretical basis of some empirical relations in seismology. *Bulletin of the Seismological Society of America*, *65*, 1073–1095.
Kearey, P., & Brooks, M. (1991). *An introduction to geophysical exploration*, (2nd ed.p. 254). Oxford: Blackwell Scientific Publications.
Kebeasy, R. M., & Gharib, A. A. (1991). Active fault and water loading are important factors in triggering earthquake activity around Aswan Lake. *Journal of Geodynamics*, *14*, 73–85. https://doi.org/10.1016/0264-3707(91)90010-C
King, G. C. P., Stein, R. S., & Lin, J. (1994). Static stress changes and the triggering of earthquakes. *Bulletin of the Seismological Society of America*, *84*, 935–953.
Loperfido, A (1919). Indagini astronomiche e geodetiche nell'area del terremoto marsicano [in Italian]. Atti Lavori Pubblici, p. 95.
Luttrell, K., & Sandwell, D. (2010). Ocean loading effects on stress at near shore plate boundary fault systems. *Journal of Geophysical Research*, *115*, B08411. https://doi.org/10.1029/2009JB006541
Neuzil, C. E. (2003). Hydromechanical coupling in geologic processes. *Hydrogeology Journal*, *11*(1), 41–83. https://doi.org/10.1007/s10040-002-0230-8
Oddone, E. (1915). Gli elementi fisici del grande terremoto Marsicano-Fucense del 13 Gennaio 1915 [in Italian]. *Bolletino della Società Sismologica Italiana*, *19*, 71–216.
Patacca, E., Scandone, P., Di Luzio, E., Cavinato, G. P., & Parotto, M. (2008). Structural architecture of the central Apennines, interpretation of the CROP 11 seismic profile from the Adriatic coast to the orographic divide. *Tectonics*, *27*, TC3006. https://doi.org/10.1029/2005TC001917
Piana Agostinetti, N., & Amato, A. (2009). Moho depth and *Vp/Vs* ratio in peninsular Italy from teleseismic receiver functions. *Journal of Geophysical Research*, *114*, B06303. https://doi.org/10.1029/2008JB005899
Piombo, A., Martinelli, G., & Dragoni, M. (2005). Post-seismic fluid flow and Coulomb stress changes in a poroelastic medium. *Geophysical Journal International*, *162*, 507–515. https://doi.org/10.1111/j.1365-246X.2005.02673.x
Rice, J. R., & Cleary, M. P. (1976). Some basic stress diffusion solutions for fluid-saturated elastic porous-media with compressible constituents. *Reviews of Geophysics*, *14*(2), 227–241. https://doi.org/10.1029/RG014i002p00227
Rovida, A., Locati, M., Camassi, R., Lolli, B., & Gasperini, P. (Eds.) (2016). CPTI15, the 2015 version of the parametric catalogue of Italian earthquakes. *Istituto Nazionale di Geofisica e Vulcanologia*. https://doi.org/10.6092/INGV.IT-CPTI15
Shen, Z.-K., Wang, M., Zeng, Y., & Wang, F. (2015). Optimal interpolation of spatially discretized geodetic data. *Bulletin of the Seismological Society of America*, *105*, 2117–2127. https://doi.org/10.1785/0120140247
Socciarelli, A. M. (2016). I terremoti nella Marsica precedenti il 1915 nella documentazione d'archivio. *Quaderni di Geofisica*, *132*, 28.
Stein, R. S. (1999). The role of stress transfer in earthquake occurrence. *Nature*, *402*, 605–609.
Stucchi, M., & Albini, P. (2000). Quanti terremoti distruttivi abbiamo perso nell'ultimo millennio? Spunti per la definizione di un approccio storico alla valutazione della completezza. In *Le ricerche del GNDT nel campo della pericolosità sismica (1996-1999)* (pp. 333–343). Roma: CNR-Gruppo Nazionale Difesa dai Terremoti.
Stucchi, M., Albini, P., Mirto, C., & Rebez, A. (2004). Assessing the completeness of Italian historical earthquake data. *Annales de Geophysique*, *47*, 659–673.
Tertulliani, A., Cucci, L., Rossi, A., & Castellano, C. (2017). Tracking earthquakes in documentary sources of the sixteenth-eighteenth centuries: Examples from Calabria (southern Italy). *Seismological Research Letters*, *88*(1), 159–170. https://doi.org/10.1785/0220160146
Toda, S., & Stein, R. S. (2002). Response of the San Andreas fault to the 1983 Coalinga-Nuñez earthquakes: An application of interaction-based probabilities for Parkfield. *Journal of Geophysical Research*, *107*(B6), 2126. https://doi.org/10.1029/2001JB000172
Tuan, T. A., Rao, N. P., Gahalaut, K., Trong, C. D., Dung, L. V., Chien, C., & Mallika, K. (2017). Evidence that earthquakes have been triggered by reservoir in the Song Tranh 2 region, Vietnam. *Journal of Seismology*, *21*, 1131–1143. https://doi.org/10.1007/s10950-017-9656-2
Wang, H. F. (2000). *Theory of linear poroelasticity with applications to geomechanics and hydrogeology* (p. 287). Princeton, NJ: Princeton University Press.
Ward, S. N., & Valensise, G. (1989). Fault parameters and slip distribution of the 1915 Avezzano, Italy, earthquake derived from geodetic observations. *Bulletin of the Seismological Society of America*, *79*, 690–710.
Yerkes, R. F., Ellsworth, W. L., & Tinsley, J. C. (1983). Triggered reverse fault and earthquake due to crustal unloading, northwest Transverse Ranges, California. *Geology*, *11*, 287–291.